Journal of Solid State Chemistry 184 (2011) 516–522

Contents lists available at ScienceDirect

Journal of Solid State Chemistry

journal homepage: www.elsevier.com/locate/jssc

Synthesis, crystal and electronic structure, and physical properties of the new lanthanum copper telluride $La_3Cu_5Te_7$

Mariya Zelinska, Abdeljalil Assoud, Holger Kleinke *

Department of Chemistry, University of Waterloo, Waterloo, ON, Canada N2L 3G1

ARTICLE INFO

Article history:
Received 18 August 2010
Received in revised form
14 December 2010
Accepted 2 January 2011
Available online 8 January 2011

Keywords:
Lanthanum
Copper
Telluride
Crystal structure
Electronic structure
Semiconductor

ABSTRACT

The new lanthanum copper telluride $La_3Cu_{5-x}Te_7$ has been obtained by annealing the elements at 1073 K. Single-crystal X-ray diffraction studies revealed that the title compound crystallizes in a new structure type, space group *Pnma* (no. 62) with lattice dimensions of $a=8.2326(3)$ Å, $b=25.9466(9)$ Å, $c=7.3402(3)$ Å, $V=1567.9(1)$ Å^3, $Z=4$ for $La_3Cu_{4.86(4)}Te_7$. The structure of $La_3Cu_{5-x}Te_7$ is remarkably complex. The Cu and Te atoms build up a three-dimensional covalent network. The coordination polyhedra include trigonal $LaTe_6$ prisms, capped trigonal $LaTe_7$ prisms, $CuTe_4$ tetrahedra, and $CuTe_3$ pyramids. All Cu sites exhibit deficiencies of various extents. Electrical property measurements on a sintered pellet of $La_3Cu_{4.86}Te_7$ indicate that it is a *p*-type semiconductor in accordance with the electronic structure calculations.

1. Introduction

Chalcogenides have been investigated for a long time due to their structural diversity [1,2] and various applications. These include semiconductor devices, e.g. in solid state electronics [3], fast-ion conductors [4,5], rechargeable batteries [6] and data storage devices including phase-change materials [7–9], chalcogenide glasses [10], and mostly tellurides for the thermoelectric energy conversion [11–14]. Examples of 3*d*/4*f* compounds, although not chalcogenides, with interesting properties include the industrially important materials Nd:YIG [15] and the permanent magnetic intermetallics $SmCo_5$ and $Nd_2Fe_{14}B_{11}$ [16] as well as the heavy fermion conductors $CeRu_2Si_2$ [17] and $HoNi_2B_2C$ [18].

Investigations of copper tellurides often revealed Cu deficiencies [19,20]. Nonstoichiometry is sometimes viewed as a nuisance in the characterization of solid state compounds, but it provides an opportunity to study how properties change as a function of composition and structure. A few copper tellurides with *f* elements have been characterized in the past, including $LnCu_{0.28}Te_2$ [21], $EuCu_{0.66}Te_2$ [22], $LnCu_xTe_2$ (*Ln*=La, Nd, Sm, Gd, Dy) [23], $Gd_3Cu_2Te_7$ [24], $U_2Cu_{0.7}Te_6$ [24], $TbCu_{0.34}Te_2$ [25], $Er_7Cu_3Te_{12}$ [26], $ErCu_3Te_3$ [27] and Th_2CuTe_6 [28]. This paper presents our study of the new ternary rare-earth copper telluride $La_3Cu_{5-x}Te_7$, with the goal to shed more light onto this area of rare-earth transition-metal tellurides.

2. Experimental section

2.1. Syntheses and analyses

The following elements, stored in a glove box under argon, were used for the syntheses: La (Alfa Aesar, 99.9%), Cu (Alfa Aesar, 99.9%), Te (Alfa Aesar, 99.999%). Shiny black needle-like crystals of the new copper telluride were first found in sample starting from La, Cu and Te in the 1:2:3 ratio. The elements were loaded into a graphite crucible and then placed into a silica tube in an argon-filled gloved box, which was then sealed under dynamic vacuum. The fused tube was placed into a resistance furnace, heated to 1173 K within 24 h, and kept at that temperature for 6 h, followed by cooling down to 973 K within 24 h, and kept at that temperature for 100 h. Thereafter, the furnace was slowly cooled to 473 K for 200 h, followed by switching off the furnace.

The reaction mixture was ground and analyzed by means of X-ray powder diffraction (INEL diffractometer with position-sensitive detector (Cu–$K\alpha_1$ radiation)). The X-ray powder diffractogram revealed that no known materials were present, indicating the formation of at least one new material. A single crystal was selected for the structure determination as described later. Subsequently, the main product was identified to be $La_3Cu_{5-x}Te_7$.

* Corresponding author.
E-mail address: kleinke@uwaterloo.ca (H. Kleinke).

0022-4596/$ - see front matter © 2011 Elsevier Inc. All rights reserved.
doi:10.1016/j.jssc.2011.01.002

A test reaction without the graphite crucible yielded the same major product, but showed some tube attack so that the use of the protecting crucible is recommended. This test provided evidence that the presence of carbon is not required for the formation of the target phase.

Then, we tried to obtain phase pure samples and to determine the phase width of $La_3Cu_{5-x}Te_7$. Samples of nominal composition $La_3Cu_{5-x}Te_7$ with $x=0$, 0.14, 0.25 and 0.5 were subsequently prepared starting from the elements in the respective ratios. The reaction mixtures were heated in graphite crucibles, encapsulated in fused silica tubes, to 773 K within 48 h, then kept at 773 K for 12 h to allow the then molten tellurium to react. Then, the tubes were heated to 1323 K within 96 h to achieve molten samples, kept at 1323 K for 48 h, then cooled down to 1073 K within 24 h. Finally, the tube was annealed at 1073 K for 14 days, followed by switching off the furnace. After this procedure, all samples were analyzed utilizing the above-mentioned X-ray powder diffractometer. The only single phase sample of $La_3Cu_{5-x}Te_7$ was obtained when $x=0.14$, common side products were $Cu_{2-x}Te$, $LaCu_{1-x}Te_2$ and $LaTe_2$. Therefore, the phase range of $La_3Cu_{5-x}Te_7$ is concluded to be smaller than $0<x<0.25$. Lower and upper ends of the phase width of $La_3Cu_{5-x}Te_7$ were established from structure refinements based on the X-ray single crystal diffraction data collected on a Bruker APEX CCD diffractometer at 295 K using ω scans. Attempts to substitute Cu with Ag and Au did not lead to the formation of the $La_3Cu_{5-x}Te_7$ type, but to binary La, Ag and/or Au tellurides.

Scanning electron microscopy was performed using the electron microscope LEO 1530 with an additional EDAX device, EDAX Pegasus 1200 (EDAX: energy dispersive analysis of X-rays). For sample with the nominal composition $La_3Cu_{4.86}Te_7$, the La/Cu/Te ratio was determined to be 20.1:33.3:46.6 (in atomic%), respectively, averaged over several crystals, which compares nicely with the nominal atomic% ratio of 20.2:32.7:47.1. No impurity elements (e.g., Si stemming from the reaction container) were detected.

In order to determine the melting point of $La_3Cu_{5-x}Te_7$ and to check for possible phase transitions, a differential scanning calorimetry (DSC) measurement was performed on the ground crystalline $La_3Cu_{4.86}Te_7$ sample with the computer controlled NETZSCH STA 409PC thermal analyzer. The measurements were carried out with a heating rate of 20 K/min and then cooled at the same rate under a constant flow of Argon (40 ml/min), which also protected the balance (flow of 30 ml/min). One prominent peak in the DSC of $La_3Cu_{5-x}Te_7$ indicates its melting point to be at 1292 K (Fig. S1 in Supporting Information).

2.2. Crystal structure determinations

A black needle-shaped crystal from the sample with the nominal composition "$LaCu_2Te_3$", later called crystal II, was selected under an optical microscope and then mounted on a glass fiber for the structure determination.

Single crystal X-ray diffraction data were collected with the use of graphite-monochromatized Mo $K\alpha$ radiation ($\lambda=0.71073$ Å) at 298 K on a Bruker APEX CCD diffractometer. The scans of 0.3° in ω were done in two groups of 606 frames with an exposure time of 60 s at $\varphi=0°$ and at $\varphi=90°$. The data were corrected for Lorentz and polarization effects. An absorption correction was performed based on fitting a function to the empirical transmission surface as sampled by multiple equivalent measurements using SADABS [29].

The lattice parameters pointed towards the orthorhombic crystal system, and the systematic absences were in accord with the space group *Pnma*. The reciprocal space images, extracted from the CCD data, were free of super cell reflections and diffuse streaks. The structure model was obtained by direct methods and refined by full-matrix least-square refinement based on F^2 using the SHELXTL5.12 package [30]. The structure solution in this space group was successful, yielding 11 independent atom sites. These sites were identified as two La, four Te and five Cu positions. The subsequent refinement revealed large thermal expansion parameters in case of all Cu sites, most notably so for Cu4 and Cu6: $U_{eq}(Cu4)=0.9$ Å^2, $U_{eq}(Cu6)=0.2$ Å^2, which were also highly anisotropic, with $U_{33}\approx U_{22}\approx 5\ U_{11}$. In addition, the final electron density map was not featureless ($\Delta\rho_{max}=15.6$ e/Å^3, $\Delta\rho_{min}=-9.07$ e/Å^3). Refining the occupancies for all five Cu sites lowered R1 from 0.091 to 0.037 (all data). A distinct maximum of 4.4 e/Å^3 in the residual electron density, surrounded by three Te atoms at a distance of 2.6 Å, pointed to the existence of a sixth deficient Cu site. After refining this site as such, R1 was decreased to 0.035 (all data), the electron density map appeared to be

Table 1
Crystallographic data for $La_3Cu_{5-x}Te_7$.

Refined formula	$La_3Cu_{4.93(5)}Te_7$, I	$La_3Cu_{4.86(4)}Te_7$, II	$La_3Cu_{4.86(7)}Te_7$, III	$La_3Cu_{4.86(7)}Te_7$, IV, HT	$La_3Cu_{4.88(7)}Te_7$, IV, LT
Formula weight [g/mol]	1622.9	1618.9	1619.1	1618.4	1620.2
T of measurement [K]	298(2)	298(2)	298(2)	298(2)	200(2)
λ [Å]	0.71073	0.71073	0.71073	0.71073	0.71073
Crystal system	Orthorhombic	Orthorhombic	Orthorhombic	Orthorhombic	Orthorhombic
Space group	*Pnma*	*Pnma*	*Pnma*	*Pnma*	*Pnma*
a [Å]	8.2306(9)	8.2326(3)	8.244(1)	8.2369(5)	8.2154(7)
b [Å]	25.923(3)	25.9466(9)	25.953(4)	25.946(2)	25.911(2)
c [Å]	7.3418(8)	7.3402(3)	7.354(1)	7.3422(4)	7.3326(6)
V [Å^3]	1566.5(3)	1567.9(1)	1573.3(4)	1569.2(2)	1560.9(2)
No. of formula units	4	4	4	4	4
Calculated density [g/cm^3]	6.881	6.858	6.835	6.851	6.894
Absorp. coeff. [mm^{-1}]	27.28	27.17	27.08	27.14	27.32
F(0 0 0)	2711	2704	2704	2703	2706
Crystal size [μm]	60 × 20 × 20	120 × 70 × 60	25 × 20 × 20	60 × 40 × 20	60 × 40 × 20
2θ range [deg.]	3.14–29.99	1.57–35.02	3.14–29.99	2.88–29.99	2.89–29.98
Reflections collected	11129	14907	14727	11996	11059
Independent reflections (R_{int})	2309 (0.048)	3471 (0.028)	2329 (0.077)	2335 (0.038)	2313 (0.042)
Reflections\refined parameters	2309\105	3471\105	2329\105	2335\105	2313\105
Goodness-of-fit on F^2	1.16	1.12	1.11	1.28	1.27
$R1$, $wR2$ (all data)	0.047, 0.056	0.035, 0.062	0.064, 0.077	0.049, 0.075	0.047, 0.076
Extinction coeff.	0.000165(13)	0.00056(3)	0.00026(3)	0.00037(2)	0.00028(3)
Max. diff. peak, hole [e/Å^3]	1.63, −1.64	2.10, −1.80	2.20, −2.04	1.91, −2.36	1.81, −1.85

Table 2
Refined Cu site occupancies of $La_3Cu_{5-x}Te_7$.

Site	$La_3Cu_{4.93}Te_7$, I	$La_3Cu_{4.86}Te_7$, II	$La_3Cu_{4.86}Te_7$, III	$La_3Cu_{4.86}Te_7$, IV, HT	$La_3Cu_{4.88}Te_7$, IV, LT
Cu1	0.063(4)	0.051(3)	0.062(5)	0.045(5)	0.099(6)
Cu2	0.697(4)	0.677(3)	0.688(5)	0.690(6)	0.639(6)
Cu3	0.800(4)	0.799(3)	0.787(5)	0.800(6)	0.790(6)
Cu4	0.183(5)	0.179(4)	0.182(6)	0.188(7)	0.208(6)
Cu5	0.435(4)	0.429(3)	0.437(6)	0.427(6)	0.384(6)
Cu6	0.285(4)	0.296(3)	0.276(6)	0.278(6)	0.324(6)

featureless, and the occupancy of this site (later called Cu1) was refined to a significant value of 5.1(3)%. The formula was refined to $La_3Cu_{4.86(4)}Te_7$.

Studying all measured reflections in reciprocal space, viewed along a^*, b^*, and finally c^* did not reveal any systematic twinning or an intergrowth crystal. In the end, the positions were standardized with the TIDY program within the PLATON package [31]. Crystallographic details are presented in Table 1. The occupancy factors of the Cu sites were refined to the values listed in Table 2.

In order to study the existence of a phase range of $La_3Cu_{5-x}Te_7$, mobility of Cu atoms and whether or not the Cu deficient sites are present in all cases, data for three more crystals were collected. One crystal was extracted from a sample of nominal composition "$La_3Cu_{5.0}Te_7$", crystal I, and two from two different samples with the same nominal compositions "$La_3Cu_{4.86}Te_7$", crystal III and crystal IV. Crystal I was analyzed in order to estimate the possible upper end point of the phase range, and crystal III in order to confirm the refinement results of crystal II. In addition to this, the crystal IV was analyzed at 298 K and at low temperature (200 K) in order to gain insight into the behavior of the Cu atoms at different temperatures. All three datasets showed comparable results with regard to the Cu deficiency, with refined formulas of $La_3Cu_{4.93(5)}Te_7$, (crystal I), $La_3Cu_{4.86(7)}Te_7$ (crystal III) and $La_3Cu_{4.86(7)}Te_7$ at 298 K (crystal IV, called HT for high temperature) and $La_3Cu_{4.88(7)}Te_7$ at 200 K (crystal IV, LT for low temperature). In fact, all formulas are equivalent within their standard deviations. Further details of the crystal structure investigations can be obtained from the Fachinformationszentrum Karlsruhe, 76344 Eggenstein-Leopoldshafen, Germany (fax: +49 7247 808 666; e-mail: crysdata@fiz-karlsruhe.de) on quoting the depository numbers CSD-422051 (crystal I), 442052 (II), 422053 (III), 422054 (IV-HT) and 422055 (IV-LT).

2.3. Electronic structure calculations

Linear Muffin Tin Orbitals (LMTO) band structure calculations [32,33] were carried out in order to understand the electronic structure of $La_3Cu_{5-x}Te_7$. In the LMTO approach, the density functional theory is used with the local density approximation (LDA) [34]. The integrations in k space were performed by an improved tetrahedron method on 252 independent k points on a grid of 576 k points evenly spread throughout the first Brillouin zone [35]. The following wave functions were used: for La 6*s*, 5*d* and 4*f*, and 5*p* downfolded [36], for Cu 4*s*, 4*p* and 3*d*; and for Te 5*s*, 5*p*, and 5*d* and 4*f* (the latter two downfolded). The structural parameters were taken from the refinement on crystal I ($La_3Cu_{4.93}Te_7$). The majority sites, Cu2 and Cu3, were treated as fully occupied and Cu5 as half occupied (model formula $La_3Cu_5Te_7$). This model requires a symmetry reduction from *Pnma* to $Pmn2_1$. In order to provide insight into the strength of various interactions, crystal orbital Hamilton populations [37] were calculated in addition to the band structures and densities of states.

2.4. Physical property measurements

A cold bar-shaped pressed pellet of the dimensions $6 \times 1 \times 1$ (in mm) from a sample of the nominal composition $La_3Cu_{4.86}Te_7$ was prepared for the measurements. In order to achieve as dense pellet as possible, the thoroughly ground phase pure sample was pressed using a force of 4 kN with a hydraulic press from Weber Pressen, corresponding to a pressure of 670 MPa. After annealing at 973 K for three days, the density was 85% of the theoretical maximum as determined via the single crystal structure studies. The Seebeck coefficient, S, and the electrical conductivity, σ, were measured simultaneously under a low pressure helium atmosphere on the commercial apparatus ULVAC-RIKO ZEM-3 in the temperature range from 300 to 620 K. The Seebeck coefficient was measured with temperature gradients of 10, 15 and 20 K at each temperature step. The temperature difference was determined via a thermocouple measurement. The specific electrical conductivity was measured using a four-point method within the ZEM-3. A powder diagram was taken after this measurement on a ground part of the pellet, and it revealed no changes.

Thermal diffusivity, D, was determined using the FlashLine 3000 thermal diffusivity system from ANTER corporation, where the flash is generated from a Xenon discharge lamp. In the flash diffusivity method, the bottom face of a disk-shaped plane-parallel sample (here: 8 mm diameter; 1 mm thickness, prepared like the bar-shaped pellet described above) is heated by the short flash. The thermal diffusivity is then determined from the time dependence of the temperature rise on the sample's top surface using an infrared detector. Thermal conductivity, κ, was determined via $\kappa = DC_P\rho$. The density, ρ, was calculated from the sample's dimensions and mass, and the specific heat, C_P, from the Dulong–Petit limit.

3. Results and discussion

3.1. Crystal structure

The new ternary telluride $La_3Cu_{5-x}Te_7$ crystallizes in own structure type. The crystal structure of $La_3Cu_{5-x}Te_7$ is shown in a projection along the c axis in Fig. 1, wherein La–Te bonds are omitted for clarity. Structure motifs include trigonal $LaTe_6$ prisms, monocapped trigonal $LaTe_7$ prisms, $CuTe_4$ tetrahedra and $CuTe_3$ pyramids.

The La1 atom is located in a monocapped trigonal prism formed by seven Te atoms with distances in the range of 3.25–3.44 Å (values here and in the following taken from the 298 K data from $La_3Cu_{4.86}Te_7$, crystal IV, Table 3). The La2 atom is in the center of a trigonal prism with six La–Te distances within the range 3.22–3.27 Å. Such distances and coordination environments are common among lanthanum tellurides, e.g. in $LaTe_2$ [38] and LaTe [39] with La–Te bonds distances between 3.22 and 3.40 Å. These distances are also comparable to the La–Te bonds of eightfold coordinated La atoms in $LaCu_{0.28}Te_2$ [21] and $LaCu_{0.40}Te_2$ [23] with bond lengths between 3.19 and 3.36 Å.

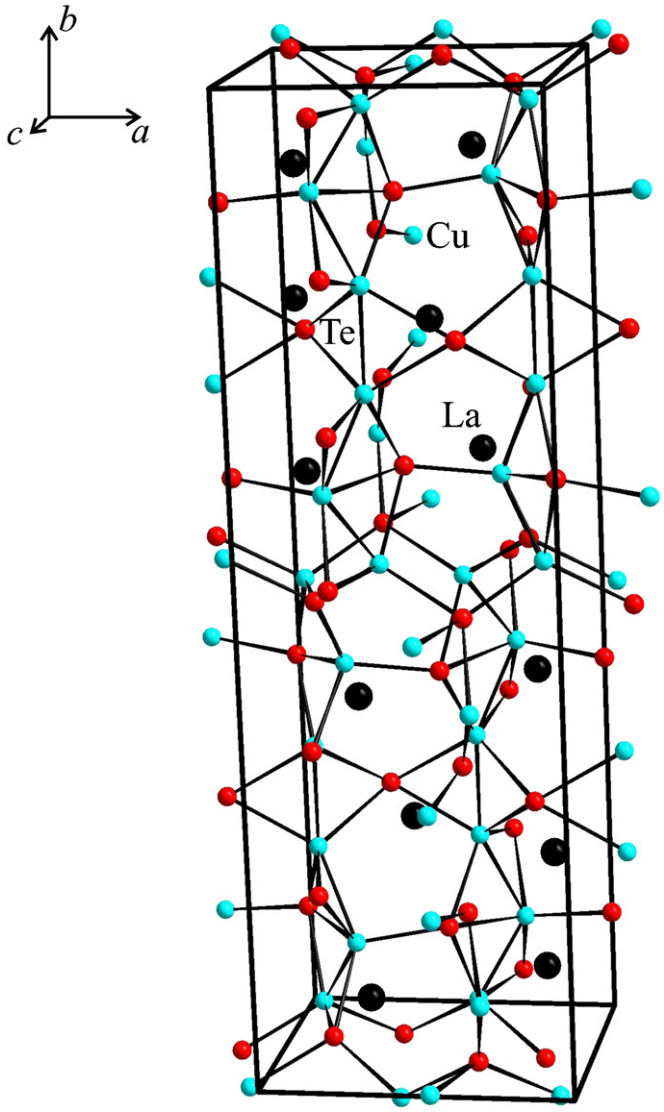

Fig. 1. Crystal structure of $La_3Cu_{5-x}Te_7$.

Several distances between the disordered Cu sites necessitate that they are never occupied at the same location within a given crystal. These distances are $d_{Cu1-Cu2}=2.33$ Å, $d_{Cu2-Cu6}=1.64$ Å, $d_{Cu3-Cu4}=1.34$ Å, $d_{Cu4-Cu5}=1.79$ Å and $d_{Cu5-Cu6}=1.27$ Å. Thus, possible oligomeric units are composed of Cu1, Cu4 and Cu6 (group 1); and Cu2, Cu3 and Cu5 (group 2). Such Cu site deficiencies are often observed in copper tellurides, for example in $Cu_{2-\delta}Te$ [40], $Ba_3Cu_{17-x}(Se,Te)_{11}$ [41] and $LaCu_{0.28}Te_2$ [21].

The first group of Cu atoms consists of Cu1, Cu4 and Cu6 with small occupancies, namely 5%, 19% and 28%, respectively. These atoms form Cu_6 zigzags chains with Cu–Cu distances ranging from 2.55 to 2.83 Å (Fig. 2a). The second group of Cu atoms comprises higher populated sites, namely Cu2, Cu3 and Cu5 with occupancies 69%, 80% and 43%, respectively. Those atoms also form Cu_6 chains, namely with distances varying from 2.55 to 2.74 Å (Fig. 2b). These Cu–Cu distances are comparable with other Cu–Cu bonds, which exist in binary CuTe (2.67 Å) [42], $Cu_{1.8}Te$ (2.64 Å–2.76 Å) [40] and ternary $Ba_3Cu_{14-\delta}Te_{12}$ (2.51 Å–2.90 Å) [43].

The predominately tetrahedral Te environment of all Cu sites is shown in Fig. 3(a/b). Only the Cu1 atoms are coordinated by just three Te atoms resulting in a flat $CuTe_3$ pyramid. The interconnections of the $CuTe_3$ and $CuTe_4$ units are made via common edges. The threefold coordination is less common for Cu, but exists for example

Table 3
Selected interatomic distances [Å] of $La_3Cu_{4.86}Te_7$ (HT) and $La_3Cu_{4.88}Te_7$ (LT).

		$La_3Cu_{4.86}Te_7$ (HT)	$La_3Cu_{4.88}Te_7$ (LT)
La1–Te1	1 ×	3.2506(9)	3.2498(8)
La1–Te1	1 ×	3.3172(9)	3.3080(9)
La1–Te2	1 ×	3.2939(8)	3.2785(8)
La1–Te2	1 ×	3.2960(9)	3.2877(8)
La1–Te3	1 ×	3.2716(9)	3.2673(9)
La1–Te3	1 ×	3.2819(9)	3.2841(9)
La1–Te3	1 ×	3.4381(9)	3.4351(9)
La2–Te2	2 ×	3.2505(9)	3.2416(8)
La2–Te2	2 ×	3.2571(9)	3.2533(9)
La2–Te4	1 ×	3.221(1)	3.214(1)
La2–Te4	1 ×	3.270(1)	3.261(1)
Cu1–Te1	1 ×	2.57(2)	2.60(1)
Cu1–Te3	1 ×	2.59(2)	2.57(1)
Cu1–Te3	1 ×	2.60(2)	2.64(1)
Cu2–Te1	1 ×	2.591(2)	2.601(2)
Cu2–Te3	1 ×	2.527(2)	2.514(2)
Cu2–Te3	1 ×	2.581(2)	2.588(2)
Cu2–Te3	1 ×	2.756(2)	2.721(2)
Cu3–Te1	1 ×	2.630(2)	2.630(2)
Cu3–Te2	1 ×	2.597(2)	2.593(2)
Cu3–Te4	1 ×	2.636(2)	2.627(2)
Cu3–Te4	1 ×	2.745(2)	2.727(2)
Cu4–Te1	1 ×	2.509(9)	2.552(6)
Cu4–Te1	1 ×	2.75(1)	2.592(7)
Cu4–Te2	1 ×	2.663(9)	2.711(6)
Cu4–Te4	1 ×	2.647(9)	2.659(7)
Cu5–Te1	1 ×	2.478(3)	2.484(3)
Cu5–Te1	1 ×	2.668(3)	2.645(4)
Cu5–Te2	1 ×	2.701(3)	2.687(4)
Cu5–Te3	1 ×	2.638(3)	2.638(3)
Cu6–Te1	1 ×	2.658(5)	2.631(4)
Cu6–Te1	1 ×	2.684(5)	2.671(4)
Cu6–Te3	1 ×	2.536(5)	2.533(4)
Cu6–Te3	1 ×	2.681(6)	2.690(5)
Cu1–Cu1	1 ×	2.61(5)	2.45(2)
Cu1–Cu6	1 ×	2.83(2)	2.88(1)
Cu2–Cu5	1 ×	2.553(4)	2.552(4)
Cu3–Cu3	1 ×	2.749(4)	2.718(3)
Cu3–Cu5	1 ×	2.737(4)	2.735(4)
Cu4–Cu6	1 ×	2.70(1)	2.599(8)
Cu5–Cu2	1 ×	2.553(4)	2.552(4)
Cu5–Cu3	1 ×	2.737(4)	2.735(4)
Cu6–Cu1	1 ×	2.83(2)	2.88(1)
Cu6–Cu4	1 ×	2.70(1)	2.599(8)

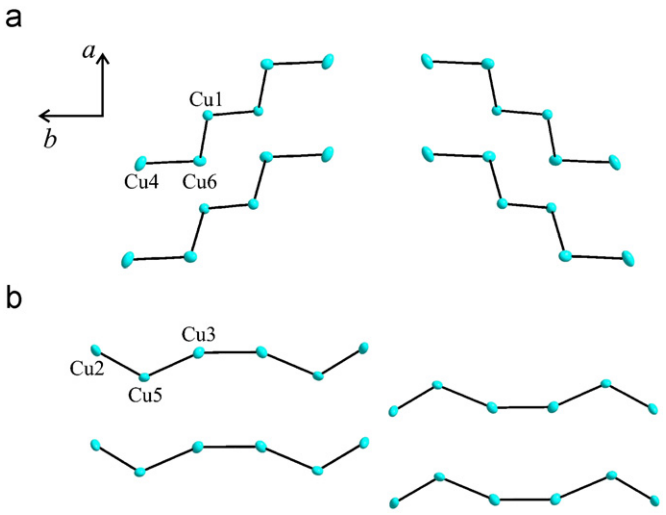

Fig. 2. Two groups of alternative Cu_6 chains of $La_3Cu_{5-x}Te_7$, comprised of (a) Cu1, Cu4, and Cu6; (b) Cu2, Cu3, and Cu5.

in $Ba_3Cu_2Sn_3Se_{10}$ [44] and $Ba_3Cu_{14-\delta}Te_{12}$ [45]. The various Cu–Te bonds between 2.51 and 2.75 Å are typical for Cu^+ and Te^{2-}.

To probe the mobility of the Cu sites, a 298 K (HT) and a 200 K (LT) structure refinement are compared. The cooling led to a volume decrease of 0.5%, with the *a* axis decreasing by 0.26% and *b* and *c* by 0.13%. The Cu site occupancies changed in part significantly while cooling, providing evidence for Cu atom mobility: for example the occupancy of Cu1 increased from 4.5(5)% to 9.9(6)%, while Cu6 increased from 27.8(6)% to 32.4(6)%. It is noted that these changes are much larger than the differences between the four different crystals at room temperature (Table 2).

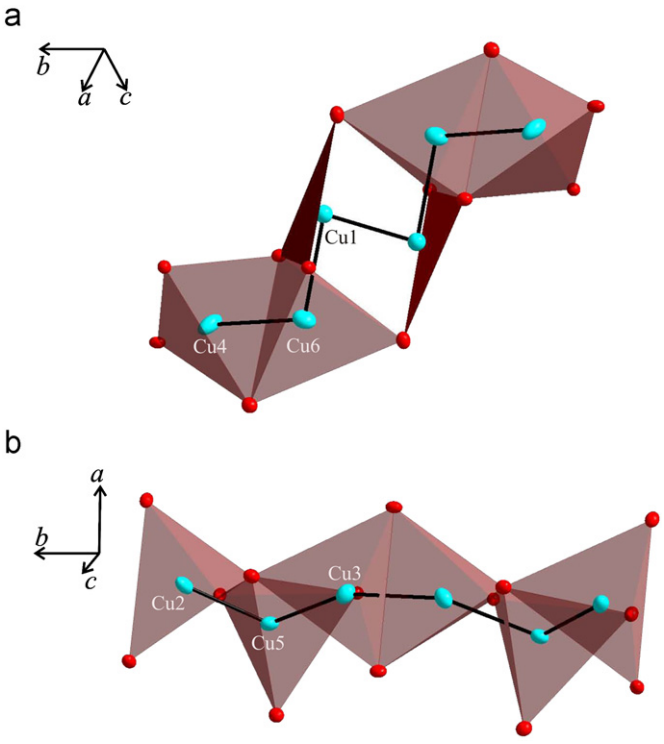

Fig. 3. The two independent Cu_6 chains with their Te coordination.

Table 4
Crystallographic positions and equivalent isotropic displacement parameters (U_{eq}) for $La_3Cu_{4.86}Te_7$ (HT) and $La_3Cu_{4.88}Te_7$ (LT).

Site	Notation	*x*	*y*	*z*	$U_{eq} \times 10^2/Å^2$
$La_3Cu_{4.88}Te_7$ (LT)					
La1	*4c*	0.13528(6)	0.59600(2)	0.44115(8)	1.16(1)
La2	*8d*	0.45457(9)	1/4	0.5527(1)	1.18(2)
Cu1	*8d*	0.0031(13)	0.5403(5)	0.0872(16)	1.0(4)
Cu2	*8d*	0.0841(2)	0.02470(8)	0.2851(3)	1.71(6)
Cu3	*8d*	0.09724(19)	0.19756(7)	0.3385(2)	1.53(5)
Cu4	*8d*	0.2441(8)	0.1627(3)	0.3212(9)	1.9(2)
Cu5	*8d*	0.2266(4)	0.1032(1)	0.4217(5)	1.6(1)
Cu6	*8d*	0.2414(5)	0.0624(2)	0.3291(6)	1.8(1)
Te1	*4c*	0.02016(7)	0.11506(3)	0.14817(9)	1.18(1)
Te2	*8d*	0.15903(7)	0.17478(2)	0.67579(8)	0.89(1)
Te3	*8d*	0.31600(7)	0.52318(2)	0.13895(9)	1.21(1)
Te4	*8d*	0.30985(10)	1/4	0.1455(1)	1.06(1)
$La_3Cu_{4.86}Te_7$ (HT)					
La1	*4c*	0.13683(7)	0.59592(2)	0.44175(8)	1.75(1)
La2	*8d*	0.45432(9)	1/4	0.5523(1)	1.69(2)
Cu1	*8d*	0.013(3)	0.5430(9)	0.090(3)	0.8(7)
Cu2	*8d*	0.0840(3)	0.02498(8)	0.2812(3)	2.80(7)
Cu3	*8d*	0.0986(2)	0.19703(7)	0.3373(2)	2.55(6)
Cu4	*8d*	0.226(1)	0.1655(4)	0.323(1)	4.5(4)
Cu5	*8d*	0.2268(4)	0.1027(1)	0.4221(5)	2.6(1)
Cu6	*8d*	0.2406(6)	0.0615(2)	0.3297(7)	2.8(2)
Te1	*4c*	0.01868(8)	0.11499(3)	0.14697(9)	1.72(2)
Te2	*8d*	0.15825(7)	0.17489(2)	0.67569(8)	1.34(1)
Te3	*8d*	0.31905(8)	0.52325(2)	0.14041(9)	1.66(2)
Te4	*8d*	0.3106(1)	1/4	0.1443(1)	1.60(2)

Moreover, especially the Cu4 atom significantly changed its position, mostly moving along the *a* axis: its *x* value increased from 0.226 to 0.244 (Table 4), which constitutes a shift of 8.22 Å × 0.018 = 0.15 Å. While almost all interatomic distances decreased after cooling to 200 K—which is the normal case, both the Cu4–Te1 and the Cu4–Te2 distances increased from 2.51 and 2.66 to 2.55 and 2.71 Å. On the other hand, the second Cu4–Te1 distance decreased very substantially from 2.75 to 2.59 Å. In addition, the changes in the equivalent isotropic displacement parameters, U_{eq}, of the different Cu sites do not all follow the same trend, in contrast to the normal behavior of the La and Te sites. Here again, the Cu4 atom stands out with its large decrease of the U_{eq} value down to 50% of its original size.

Ion exchange reaction tests with placing a $La_3Cu_{4.86}Te_7$ sample in aqueous 2N $AgNO_3$ solutions yielded a blue color after a few days, indicative of Cu ions in the solution. The microcrystalline sample mostly consisted of Ag_2Te. A test performed in water without the Ag^+ addition led to no reaction. These tests as well point towards Cu ion mobility, as demonstrated for $Ba_3Cu_{17-x}(Se,Te)_{11}$ [41] and $Cu_2P_3I_2$ [46].

3.2. Electronic structure

The density of states (DOS) of the model $La_3Cu_5Te_7$ reveals a band gap at the Fermi level, E_F (left part of Fig. 4). The Cu *d* states predominate the valence band between −5 and −3 eV, supporting the assumption of Cu^+ in this material. The remainder of the valence band is comprised mostly of Te *p* states. The electron-precise formulation is thus $(La^{3+})_3(Cu^+)_{5-x}(Te^{2-})_7$ when $x=0$. This corresponds to filled *d* states for Cu, and filled *s* and *p* states for Te. Hence, the material is predicted to be a semiconductor.

The band gap separates the filled bonding states of the Cu–Te interactions from the empty antibonding ones, while some Cu–Cu antibonding states are filled just below E_F (left and middle part of Fig. 4). The small Cu deficiency experimentally found then leads to stronger Cu–Cu bonds by depopulating the top of the valence band and hence some Cu–Cu antibonding states, compared to the $La_3Cu_5Te_7$ model.

3.3. Physical properties

The measurements were performed on a sample of nominal composition $La_3Cu_{4.86}Te_7$. $La_3Cu_{4.86}Te_7$ can be characterized as a *p*-doped semiconductor with a small positive Seebeck coefficient, varying from $S=15$ to 34 μV/K between 300 and 620 K (circles in

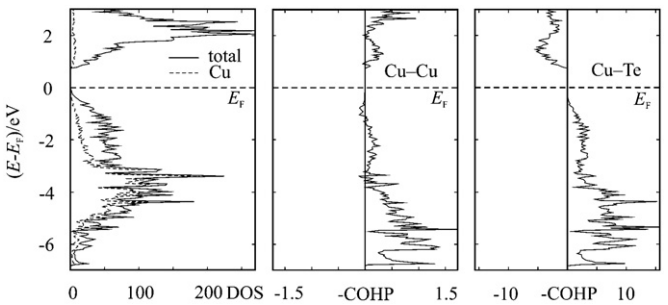

Fig. 4. Densities of states (DOS, left) and cumulated Cu–Cu (center) and Te–Te crystal orbital Hamilton populations (COHP, right) of the $La_3Cu_5Te_7$ model. The Fermi level, E_F, was arbitrarily placed at 0 eV.

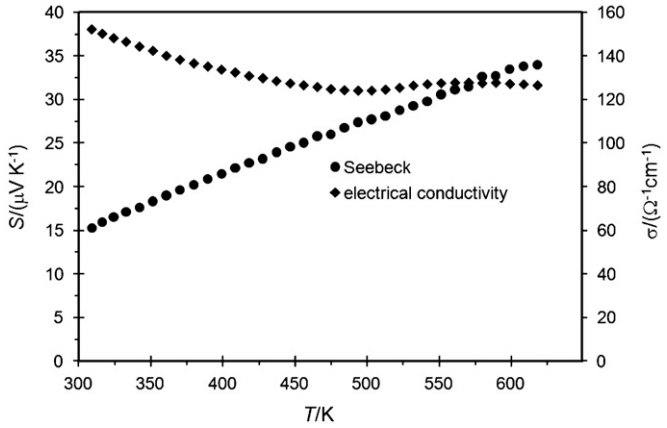

Fig. 5. Seebeck coefficient (circles) and electrical conductivity (diamonds) of $La_3Cu_{4.86}Te_7$.

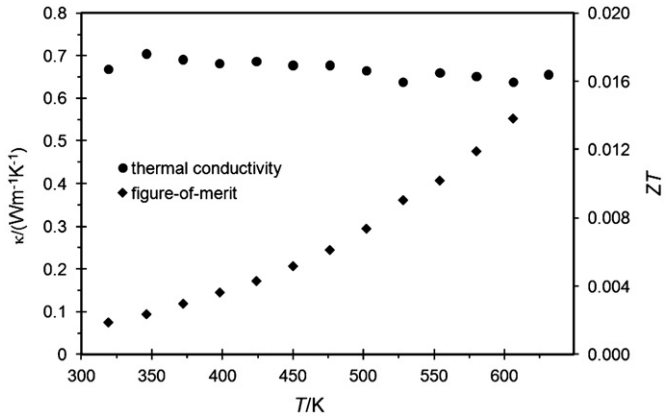

Fig. 6. Thermal conductivity (circles) and figure-of-merit (diamonds) of $La_3Cu_{4.86}Te_7$.

Fig. 5). The electrical conductivity, σ, decreases slowly with increasing temperature from approximately 150 Ω^{-1} cm^{-1} at 300 K to 120 Ω^{-1} cm^{-1} at 620 K, typical for a heavily doped semiconductor, as the charge carrier concentration is basically independent of the temperature (diamonds in Fig. 5). The slight upwards trend, commencing around 530 K, is indicative of a slight charge carrier increase, as that temperature suffices for the carriers to cross the band gap.

The thermal conductivity, κ, is basically independent of the temperature, with values around 0.7 Wm^{-1} K^{-1} (circles in Fig. 6). The electrical contribution, κ_{el}, to the overall thermal conductivity of $La_3Cu_{4.86}Te_7$ at room temperature is estimated to be 0.12 Wm^{-1} K^{-1}, according to the Wiedemann–Franz law $\kappa_{el}=L\sigma T$, with the Lorenz number $L=2.44\times10^{-8}$ W Ω K^{-2} [47] and $\sigma=150\,\Omega^{-1}$ cm^{-1}. This leaves the lattice contribution, $\kappa_L=\kappa-\kappa_{el}=0.58$ Wm^{-1} K^{-1}. The thermal conductivity of the new telluride is even lower than those in the recently characterized $Cs_2BaCu_8Te_{10}$ (1.2 Wm^{-1} K^{-1}) and $Rb_2BaCu_8Te_{10}$ (1.4 Wm^{-1} K^{-1}) [48] and in most filled skutterudites, a class of materials with high potential for thermoelectric applications [49,50]. Such a small number, though in part caused by the low density of the pressed pellet, is a consequence of the low symmetry of $La_3Cu_{5-x}Te_7$ and its Cu atom disorder.

The thermoelectric figure-of-merit, $ZT=TS^2\sigma/\kappa$, of $La_3Cu_{5-x}Te_7$ increases from 0.002 at 309 K to 0.014 at 618 K (diamonds in Fig. 6). Because the thermal conductivity was measured at different temperatures than the Seebeck coefficient and the electrical conductivity, a polynominal fit of the power factor ($S^2\sigma$) combined with the measured thermal conductivity (κ) was used to determine ZT. The uncertainty of the ZT values is estimated to be around 7%. For comparison, advanced thermoelectrics may exhibit or even exceed $ZT=1$ [48,51–53]. While using a pellet with higher relative density will likely lead to higher values, this material will still not be competitive. Furthermore, the mobility of the Cu ions is expected to cause stability problems in the long run.

4. Conclusions

A new ternary telluride, $La_3Cu_{5-x}Te_7$, with $x\approx0.1$, was discovered and characterized. No evidence for a significant phase range was found. This telluride adopts a new structure type with a three-dimensionally extended covalent Cu–Te network. Therein, all Cu sites are deficient, enabling Cu ion mobility.

In accord with the electronic structure calculations, $La_3Cu_{5-x}Te_7$ is a *p*-doped semiconductor. Its small Seebeck coefficient as well as its Cu ion mobility stands against its use as a thermoelectric material.

Acknowledgments

Financial support from NSERC, CFI, OIT (Ontario Distinguished Researcher Award for H.K.), and the Canada Research Chair program (CRC for H.K.) is appreciated.

Appendix A. supporting Information

Supplementary data associated with this article can be found in the online version at doi:10.1016/j.jssc.2011.01.002.

References

[1] P. Böttcher, Angew. Chem. Int. Ed. Engl. 27 (1988) 759–772.
[2] C. Graf, A. Assoud, O. Mayasree, H. Kleinke, Molecules 14 (2009) 3115–3131.
[3] L.L. Kosbar, C.E. Murray, M. Copel, A. Afzali, D.B. Mitzi, Nature 428 (2004) 299–303.
[4] S. Lange, T. Nilges, Chem. Mater. 18 (2006) 2538–2544.
[5] N. Zheng, X. Bu, P. Feng, Nature 426 (2003) 428–432.
[6] J.-M. Tarascon, M. Armand, Nature 414 (2001) 359–367.
[7] G. Atwood, Science 321 (2008) 210–211.
[8] D. Lencer, M. Salinga, B. Grabowski, T. Hickel, J. Neugebauer, M. Wuttig, Nat. Mater. 7 (2008) 972–977.
[9] N. Yamada, M. Wuttig, Nat. Mater. 6 (2007) 824–832.
[10] A. Zakery, S.R. Elliott, J. Non-Cryst. Solids 330 (2003) 1–12.
[11] N.D. Lowhorn, T.M. Tritt, E.E. Abbott, J.W. Kolis, Appl. Phys. Lett. 88 (2006) 022101/022101–022101/022103.
[12] D.M. Rowe, Thermoelectrics Handbook: Macro to Nano, CRC Press, Taylor & Francis Group, Boca Raton, FL, USA, 2006.
[13] J.R. Sootsman, H. Kong, C. Uher, J.J. D'Angelo, C.-I. Wu, T.P. Hogan, T. Caillat, M.G. Kanatzidis, Angew. Chem. Int. Ed. 47 (2008) 8618–8622.
[14] H. Xu, K.M. Kleinke, T. Holgate, H. Zhang, Z. Su, T.M. Tritt, H. Kleinke, J. Appl. Phys. 105 (2009) 053703/053701–053703/053705.
[15] J. Helszan, YIG Resonators and Filters, John Wiley & Sons, New York, 1985.
[16] J.F. Herbst, Rev. Mod. Phys. 63 (1991) 819–898.
[17] S. Raymond, J.P. Rueff, S.M. Shapiro, P. Wochner, F. Sette, P. Lejay, Solid State Commun. 118 (2001) 473–477.
[18] A.I. Goldman, C. Stassis, P.C. Canfield, J. Zaretsky, P. Dervenagas, B.K. Cho, D.C. Johnston, B. Sternlieb, Phys. Rev. B 50 (1994) 9668–9671.
[19] O.P. Astakhov, Neorg. Mater. 11 (1975) 23–27.
[20] B. Mansour, F. Mukhtar, G.G. Barakati, Phys. Status Solidi 95 (1986) 703–707.
[21] N.H. Dung, M.P. Pardo, P. Boy, Acta Cryst. C 39 (1983) 668–670.
[22] R. Patschke, P. Brazis, C.R. Kannewurf, M.G. Kanatzidis, J. Mater. Chem. 9 (1999) 2293–2296.
[23] F.Q. Huang, P. Brazis, C.R. Kannewurf, J.A. Ibers, J. Am. Chem. Soc. 122 (2000) 80–86.
[24] F.Q. Huang, J.A. Ibers, J. Solid State Chem. 159 (2001) 186–190.
[25] L.D. Gulay, I.D. Olekseyuk, J. Solid State Chem. 387 (2005) 154–159.
[26] L.D. Gulay, I.D. Olekseyuk, A. Pietraszko, 403 (2005) 223–227.
[27] L.D. Gulay, D. Kaczorowski, J. Alloys Compd. 422 (2006) 16–20.
[28] A.A. Narducci, J.A. Ibers, Inorg. Chem. 37 (1998) 3798–3801.
[29] SAINT, Madison, W1, 1995.

[30] G.M. Sheldrick, SHELXTL, Version 5.12 ed., Siemens Analytical X-Ray Systems, Madison, WI, 1995.
[31] A.L. Spek, J. Appl. Crystallogr. 36 (2003) 7–13.
[32] O.K. Andersen, Phys. Rev. B 12 (1975) 3060–3083.
[33] H.L. Skriver, The LMTO Method, Springer, Berlin, Germany, 1984.
[34] L. Hedin, B.I. Lundqvist, J. Phys. C 4 (1971) 2064–2083.
[35] P.E. Blöchl, O. Jepsen, O.K. Andersen, Phys. Rev. B 49 (1994) 16223–16233.
[36] W.R.L. Lambrecht, O.K. Andersen, Phys. Rev. B 34 (1986) 2439–2449.
[37] R. Dronskowski, P.E. Blöchl, J. Phys. Chem. 97 (1993) 8617–8624.
[38] A.A. Eliseev, V.G. Kuznetsov, Neorg. Mater. 1 (1965) 635–639.
[39] T.H. Ramsey, H. Steinfink, E.J. Weiss, Inorg. Chem. 4 (1965) 1154–1157.
[40] R.V. Baranova, A.S. Avilov, Z.G. Pinsker, Kristallografiya 18 (1973) 1169–1176.
[41] B. Kuropatwa, Y. Cui, A. Assoud, H. Kleinke, Chem. Mater. 21 (2009) 88–93.
[42] F. Pertlik, Mineral. Petrol. 71 (2001) 149–154.
[43] A. Assoud, J. Xu, H. Kleinke, Inorg. Chem. 46 (2007) 9906–9911.
[44] A. Assoud, N. Soheilnia, H. Kleinke, Chem. Mater. 17 (2005) 2255–2261.
[45] A. Assoud, S. Thomas, B. Sutherland, H. Zhang, T.M. Tritt, H. Kleinke, Chem. Mater. 18 (2006) 3866–3872.
[46] M.H. Möller, W. Jeitschko, J. Solid State Chem. 65 (1986) 178–189.
[47] L. Lorenz, Ann. Phys. Chem. 223 (1872) 429–452.
[48] R. Patschke, X. Zhang, D. Singh, J. Schindler, C.R. Kannewurf, N. Lowhorn, T. Tritt, G.S. Nolas, M.G. Kanatzidis, Chem. Mater. 13 (2001) 613–621.
[49] G.S. Nolas, D.T. Morelli, T.M. Tritt, Annu. Rev. Mat. Sci. 29 (1999) 89–116.
[50] H. Kleinke, Chem. Mater. 22 (2010) 604–611.
[51] G.J. Snyder, E.S. Toberer, Nat. Mater. 7 (2008) 105–114.
[52] D.-Y. Chung, T.P. Hogan, M. Rocci-Lane, P. Brazis, J.R. Ireland, C.R. Kannewurf, M. Bastea, C. Uher, M.G. Kanatzidis, J. Am. Chem. Soc. 126 (2004) 6414–6428.
[53] E.S. Toberer, A.F. May, G.J. Snyder, Chem. Mater. 22 (2010) 624–634.